Acidic Magnetorheological Finishing of Infrared Polycrystalline Materials

Introduction

Magnetorheological finishing (MRF) is a polishing technique used to produce high-precision optics. It is known for its relatively high material-removal rate (mrr);[1] subnanometer surface roughness on various materials, especially glass;[2–4] good figure/shape accuracy;[5] deterministic nature;[1] and the ability to polish complex shapes at a large size range.[6] For some materials, however, the conventional alkaline water-based magnetorheological (MR) fluid tends to leave noticeable artifacts and a relatively high roughness on the surface;[7–10] e.g., Jacobs *et al.*[7] talked about the difficulties in using a conventional MR fluid to polish calcium fluoride (CaF_2) and potassium dihydrogen phosphate (KDP). It was shown that since CaF_2 is a soft material [H_V = 1.65 GPa (Ref. 11)], it is easily chipped and tends to experience a large number of fine scratches. On the other hand, KDP is particularly soluble in water; therefore, any water-based MR fluid is not recommended when polishing this material. The alternative MR fluid for finishing CaF_2 was based on a lubricant component (PEG 200) instead of water to soften the MR fluid and prevent fine scratches. The magnetic-field strength on the MRF machine was also reduced to further soften the MR fluid. The results showed a root-mean-square (rms) surface roughness of ~1 nm for this material. For KDP, the water component was replaced with dicarboxylic acid ester. Surface-roughness results (when using nanodiamond as a polishing abrasive) were as low as ~20-nm peak-to-valley (p–v) and ~1.6-nm rms. Similarly, Menapace *et al.*[12] [Lawrence Livermore National Laboratory (LLNL)] successfully polished a 50 × 50-mm^2 KDP substrate using an optimized nonaqueous MR fluid. The surface microroughness achieved was in the mid-angstrom level, along with a 5× improvement in the surface figure. More recently, Pattanaik *et al.*[13] described the use of an MRF setup for polishing a nonmagnetic copper substrate using an oil-based MR fluid. By modifying both the MR fluid composition [mainly the concentration of carbonyl iron (CI), a polishing abrasive, and an oil-based medium] and the experimental setup (relative rotational movement between the workpiece and MR fluid), they found the optimal conditions at which a smooth surface roughness is achieved.

Another group of materials that is relatively challenging to finish by using MRF [and other techniques (see Refs. 14–16)] consists of crystalline[8,17] and polycrystalline materials.[9,10,18] The difficulty arises because of the material anisotropy in the unit cell regime (mostly found at the less-symmetric lattice systems, such as hexagonal) and/or in the grain-array regime.[19–21] Kozhinova *et al.*[9] (and later Hallock *et al.*[10]) demonstrated the use of an altered MR fluid to finish an infrared (IR) polycrystalline material—chemical-vapor–deposited (CVD) ZnS. They showed that when this material is processed with a conventional alkaline MR fluid, surface-artifact phenomena known as "pebbles"[9,22] (in the mesostructured regime) and "orange peel" (in the grain-structure regime)[23] are raised on the finished surface; furthermore, the more material removed by MRF, the rougher the surface. They experimented with the MRF process by using a modified MR fluid in which the CI particles were replaced with a "soft" CI type and the carrier medium was modified from alkaline to acidic. When using this type of modified MR fluid, the surface artifacts and roughness can be minimized.

In our ongoing research, we investigate the role of chemical and mechanical effects on the mrr during MRF of IR polycrystalline materials, with considerable focus on CVD ZnS. Seeking an explanation to Kozhinova's findings, we investigated[19] the anisotropy of ZnS during MRF using four dominant single-crystal orientations of ZnS (100, 110, 111, and 311). The relative mrr's between the different orientations were examined during MRF, using three chemomechanically modified MR fluids: pH 6 with viscosity (η) of ~197 cP, pH 5 with $\eta \approx 117$ cP, and pH 4 with $\eta \approx 47$ cP. We used unique CI particles coated with a thin layer of zirconia to protect the iron particles from rapid corrosion in acidic conditions.[24–26] We found that the minimal variation in the removal rate between the four crystalline orientations was obtained with a pH 4 and low-viscosity (~47-cP) MR fluid. This suggested that during MRF, most of the grains within the polycrystalline material are polished at relatively the same rate (uniformly), leaving a few surface artifacts (pebbles) and a relatively low surface roughness. When this formulation was tested on several CVD ZnS substrates, we found that

pebble artifacts were minimal with this composition; however, surface microroughness was relatively high at ~44-mm rms. The missing part in our previous work[19] was lacking polishing abrasive in the acidic MR fluid. In this article we describe our efforts to further reduce the appearance of pebbles and improve surface roughness on several CVD ZnS substrates and other important IR polycrystalline materials using an acidic, low-viscosity MR fluid. A modified version of zirconia-coated CI particles to further increase the acidic MR fluid's lifespan at pH 4.5 (Refs. 27 and 28) is used. We first examine the effect of two polishing abrasives—alumina and nanodiamond—on the removal-rate uniformity of single-crystal orientations of ZnS and then examine the surface finish of several IR polycrystalline materials that were polished with two acidic, low-viscosity MR fluids containing these two polishing abrasives.

Experimental Details

1. IR Optical Substrates

The crystalline materials and their relevant properties are listed in Table 146.IV. All single-crystal ZnS samples were grown, cut, and supplied by the same supplier.[29] Polycrystalline CVD ZnS materials were obtained from different suppliers, each providing one sample (samples A, B, C, and D in Table 146.IV). Technically the material is listed as CVD ZnS; however, differences are anticipated because of variations in detailed manufacturing conditions with each supplier.[20,30] Also, samples A–C are forward-looking IR (FLIR) ZnS, while sample D is elemental ZnS.

Hot isostatic pressed (HIP) ZnS, CVD ZnSe, and MgF_2 were also provided from different suppliers. All materials were ground and pre-polished in-house, as described in Ref. 9, to a flatness of 1 to 2 λ, a p–v roughness of <40 nm, and an rms of <4 nm.

2. Acidic MR Fluids

The MR fluids we used are based on the "advanced zirconia-coated CI particles." The particles' synthesis and characterization are widely described in Refs. 27 and 28. The use of the coated particles in an acidic suspension greatly improves the MR fluid's lifespan by suppressing oxidation of the carbonyl iron particles. The primary formulation of the acidic MR

Table 146.IV: Characteristics and properties of IR crystalline materials.

Sample ID	Sample Type	Crystal Structure	H_V (GPa)*	Grain Size (μm)
ZnS (100)	Single crystal	Cubic	1.89±0.03 (Ref. 19)	N/A
ZnS (110)	Single crystal	Cubic	1.71±0.04 (Ref. 19)	N/A
ZnS (111)	Single crystal	Cubic	2.93±0.04 (Ref. 19)	N/A
ZnS (311)	Single crystal	Cubic	2.17±0.12 (Ref. 19)	N/A
ZnS A†	Polycrystalline; CVD; FLIR	Cubic	1.86±0.02 (Ref. 28)	1.18±0.34**
ZnS B†	Polycrystalline; CVD; FLIR	Cubic	1.72±0.02 (Ref. 28)	2.03±0.64**
ZnS C‡	Polycrystalline; CVD; FLIR	Cubic	1.61±0.14 (Ref. 28)	—
ZnS D‡	Polycrystalline; CVD; elemental	Cubic	2.00±0.03 (Ref. 28)	1.94±0.46**
HIP ZnS	Polycrystalline; CVD; HIP	Cubic	1.33±0.05 (Ref. 28)	75 to 150 (Ref. 22)
ZnSe	Polycrystalline; CVD	Cubic	0.90±0.06 (Ref. 28)	43±9.00 (Ref. 31)
MgF_2	Polycrystalline	Tetragonal	2.29±0.05 (Ref. 28)	~0.45*** (Ref. 32)

*Taken with a Tukon 300 BM Micro-Indenter at 100-g force for single-crystal samples and 400-g force for all other samples.
**The lineal-intercept method for determining average grain size was used.
***An image-analyzing software was used.
†From U.S. vendors
‡From Chinese vendors

fluid, given in Table 146.V, was blended off-line using a shaft mixer. Small portions of powder were incrementally added to a mixture of water and a particle-dispersant agent [polyethylene-imine (PEI), Sigma Aldrich] to form a slurry. The acid (glacial acetic acid, Sigma Aldrich) was added last. Polishing abrasives—alumina and diamond (see Table 146.VI for more details)—were added (to separate fluids) at a different stage of the experiment, when the fluids were circulating on the MRF machine. This had no effect on the fluids' viscosity or pH value. For the alumina-based MR fluid, the abrasive concentrations evaluated, in volume percent (vol %), were 0 vol %, 1 vol %, 2 vol %, and 3 vol %. For the nanodiamond-based MR fluid, the abrasive concentrations evaluated were 0 vol %, 0.06 vol %, 0.12 vol %, and 0.18 vol %. Note that the diamond-abrasive concentration is one order of magnitude lower than that of alumina because the nanodiamond abrasive is more aggressive than alumina. The acidic MR fluids had an off-line viscosity of ~45 cP. The pH of the fluids throughout the experiments was 4.53±0.09 and 4.54±0.11 for the alumina and diamond-based fluids, respectively. One liter from each fluid was prepared and loaded on the MRF machine.

Table 146.V: Acidic MR-fluid formulation showing the different components, their original form of supply, and their relative portion in the fluid (in volume percent).

Component	Form of Supply	MR Fluid (vol %)
Advanced zirconia-coated CI particles	Powder	27.97
DI (de-ionized) water	Liquid	49.30
Polyethylene-imine	50 wt% in water	20.71
Acetic acid	~16-M solution	2.02

3. MRF Spotting Experiment

An MRF spotting experiment was conducted on a research MRF machine, referred to as the "spot-taking machine" (STM).[7] The STM has features similar to a conventional MRF machine; however, it is not designed to perform a full run of polishing. It is capable of taking single spots at a time because of a lack of part movement. An example of an MRF spot and the removal function is shown in Fig. 146.49. The acidic MR fluids (containing different abrasive types and concentrations) were used in a screening spotting experiment on single-crystal orientations of ZnS. Each single-crystal substrate was spotted twice with a given acidic fluid for 1 min. The peak removal rate (prr) was then measured. Following the screening experiment with single-crystal ZnS, the fluids with the highest abrasive concentration (i.e., 3 vol% alumina and 0.18 vol% diamond) were used in the second spotting stage of polycrystalline IR materials. Each polycrystalline substrate was spotted once for 15 min to remove between 0.7 to 1.0 μm of material at the deepest depth of penetration (ddp). The spotting time was chosen

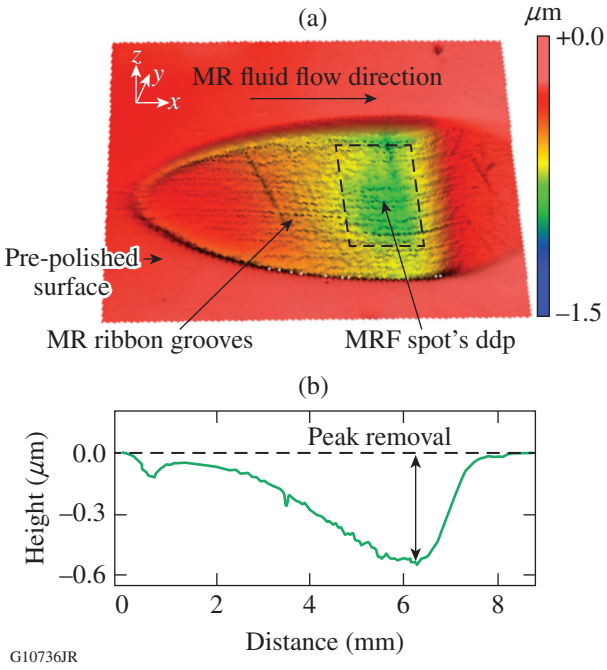

Figure 146.49
(a) A 3-D white-light interferometer image (12 × 8 mm^2) of a magnetorheological finishing (MRF) spot taken on a pre-polished chemical-vapor–deposited (CVD) ZnS substrate (sample A) designating the spot's depth of deepest penetration (ddp), MR ribbon grooves, and MR fluid-flow direction. (b) The MRF removal function shows the peak removal around the spot's ddp.

Table 146.VI: Polishing abrasives, their source, and characteristics.

Polishing Abrasive	Source	Form of Supply	Particle Size* (nm)
Alumina (alpha)	NanoTek	Dry powder	d_{15} = 19; d_{50} = 52; d_{80} = 169
DIANAN® nanodiamond	Straus Chemical	Dry powder	d_{15} = 13; d_{50} = 28; d_{80} = 143

*Particle-sized data were obtained with the AcoustoSizer IIS-Particle size and zeta potential analyzer.[33] Samples contained 0.5 wt% of abrasive in DI water. All suspensions were dispersed using a sonication bath for 20 min prior to measurement.

based on Ref. 9, which states that pebbles on a pre-polished CVD ZnS surface are exposed after ~0.5 μm of material has been removed. Machine settings were 1.3-mm ribbon height, 0.2-mm (for single crystals) and 0.3-mm (for polycrystalline) penetration depth, 220-rpm wheel speed, 110-rpm pump speed, and a 15-A electric current.

4. Metrology

a. Material removal rate of single-crystal ZnS substrates. Peak removal rates for all spots taken on the single-crystal substrates were obtained with a Zygo Mark IV laser interferometer[34] by subtracting the spotted area from the original surface and dividing the difference by the spotting time, i.e., 1 min. The peak removal is measured as the deepest vertical depth of material removed by MRF (see Fig.146.49).

b. Surface artifacts and microroughness of polycrystalline materials. The submillimeter- and millimeter-sized pebbles on the spotted polycrystalline materials, which are a direct result of the CVD growth technique,[9,22,35,36] were evaluated using a Zygo white-light, non-contact interferometer—the NewView™ 100 (Ref. 37). A 5× objective (with a 1.39 × 1.04-mm^2 field of view) was used to capture two areal-roughness measurements at the ddp of the spots. These measurements were analyzed, using a low-pass filter option in MetroPro, to screen out the roughness and leave only the surface waviness.[38] An example of a low-pass filtered measurement is given in Figs. 146.50(a)–146.50(c), where (a) the original measurement is decomposed to (b) a waviness plot and (c) a roughness plot. The waviness data provide an indication on the pebbles' severity on the surface. Surface microroughness, which captures submicron- and micron-sized features, such as pits, scratches, and grain boundaries (known as orange peel[23]), was measured using the NewView 100™ with a 20× objective (a 0.35 × 0.26-mm^2 field of view). Four areal measurements were taken at the ddp of each spot. Within each areal measurement, five lineout scans were collected in the direction of the MR fluid flow. This helps to avoid the grooves created by the MR ribbon during MRF (see Fig. 146.49), which are a direct result of the workpiece being stationary and not rotating on the STM. We believe that the lineout data better reflect the roughness one would obtain if a conventional MRF machine with a full run would have been used. All p–v and rms-roughness data were averaged and are presented in Tables 146.VII and 146.VIII for CVD ZnS and Tables 146.IX and 146.X for the other IR materials.

Results

1. Material Removal Rate of Single-Crystal ZnS

The average prr for all four single-crystal ZnS substrates finished with various amounts of alumina and diamond abrasives in the acidic MR fluids is given in Table 146.VII and Figs. 146.51(a) and 146.51(b). Both sources indicate that the addition of abrasives increased the overall prr of the acidic fluids. When alumina was first added to the acidic fluid, the average prr of all four orientations increased by ~59%—from ~0.029 μm/min to ~0.046 μm/min (see the highlighted line in Table 146.VII); when diamonds were first added to the acidic fluid, the average increased by ~46%—from ~0.026 μm/min to ~0.038 μm/min. For the acidic fluids with alumina, an additional amount of abrasive has no real effect on the prr. Observation of the data within the standard deviation shows little change in the average prr with increased abrasive concentration after the first dose is added [Fig. 146.51(a)]. For the acidic fluid containing the diamonds, however, an additional amount of abrasive linearly increases the average prr of the fluid [Fig. 146.51(b)]. The highest average prr of the fluid is achieved when 3× the amount of diamond abrasive is used—i.e., 0.18 vol %.

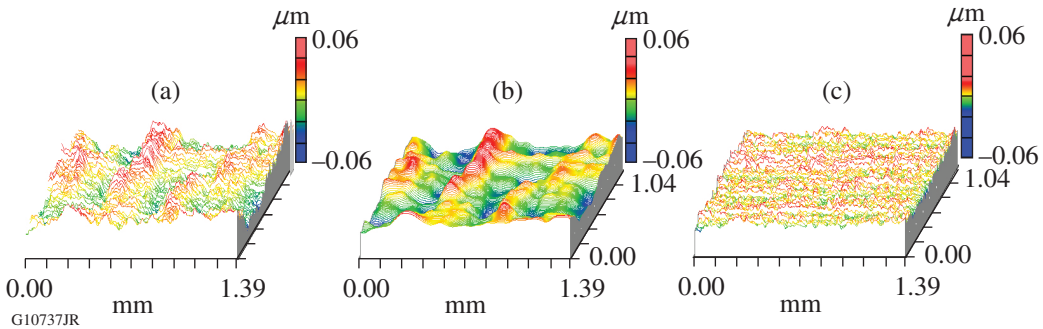

Figure 146.50
A set of 3-D white-light interferometer images (1.39 × 1.04 mm^2) of a CVD ZnS (sample A) substrate finished with a conventional alkaline MR fluid. (a) Original measurement showing both surface waviness and roughness, (b) low-pass filter analysis showing surface waviness (indication of pebbles), and (c) screened-out high-frequency roughness.

Table 146.VII: Average peak removal rate (μm/min) for single-crystal substrates of ZnS finished with acidic MR fluids that contain various amounts of alumina and nanodiamond abrasives. Note that the alumina-abrasive concentration is an order of magnitude higher than the nanodiamond.

Single-Crystal Orientation	Acidic MR Fluid with Alumina Abrasive				Acidic MR Fluid with Nanodiamond Abrasive			
	0 vol %	1 vol %	2 vol %	3 vol %	0 vol %	0.06 vol %	0.12 vol %	0.18 vol%
100	0.030±0.002	0.045±0.001	0.040±0.001	0.041±0.000	0.029±0.000	0.035±0.000	0.046±0.007	0.053±0.001
110	0.028±0.000	0.046±0.004	0.048±0.002	0.039±0.000	0.029±0.002	0.043±0.003	0.050±0.003	0.056±0.004
111	0.032±0.003	0.045±0.000	0.049±0.003	0.041±0.002	0.020±0.002	0.036±0.008	0.046±0.003	0.051±0.005
311	0.028±0.001	0.048±0.002	0.040±0.003	0.045±0.002	0.025±0.001	0.037±0.001	0.040±0.007	0.053±0.000
Average	0.029±0.002	0.046±0.001	0.044±0.005	0.042±0.002	0.026±0.004	0.038±0.004	0.046±0.004	0.053±0.002

Table 146.VIII: Surface waviness as p–v and rms collected with a 5× objective at the spots' ddp of four polycrystalline, CVD ZnS substrates provided by different suppliers. Data were obtained using a low-pass filter.

CVD ZnS Sample ID	Acidic MR Fluid with Alumina Abrasive			Acidic MR Fluid with Nanodiamond Abrasive		
	ddp (μm); removal rate (μm/min)	p–v (nm)	rms (nm)	ddp (μm); removal rate (μm/min)	p–v (nm)	rms (nm)
Sample A	0.76; 0.051	62.26±33.02	7.06±1.76	0.95; 0.063	64.51±1.31	9.24±0.86
Sample B	0.77; 0.051	54.83±13.33	7.22±1.34	0.84; 0.056	47.29±0.48	5.51±0.22
Sample C	0.69; 0.046	194.67±42.24	24.14±0.82	1.10; 0.073	55.47±.91	7.35±1.76
Sample D	0.79; 0.053	147.85±1.91	16.43±0.72	0.94; 0.063	71.46±12.43	7.81±2.34

Table 146.IX: Surface microroughness as areal and lineout p–v and rms collected with a 20× objective at the spots' ddp of four polycrystalline, CVD ZnS substrates provided by different suppliers.

Sample	Acidic MR Fluid with Alumina Abrasive				Acidic MR Fluid with Nanodiamond Abrasive			
	Areal		Lineouts		Areal		Lineouts	
	p–v (nm)	rms (nm)	p–v (nm)	rms (nm)	p–v (nm)	rms (nm)	p–v (nm)	rms (nm)
A	694.23±8.10	18.53±1.58	75.70±7.88	14.22±1.35	1361.11±147.15	14.33±1.01	28.46±4.54	6.10±1.24
B	694.68±25.87	20.38±1.79	79.39±15.19	15.58±2.75	775.50±285.04	10.32±2.54	27.66±4.38	5.93±0.76
C	903.72±110.06	39.48±1.80	111.67±52.06	29.83±4.47	1364.06±53.33	26.94±1.70	32.87±7.58	7.79±1.98
D	1160.39±343.47	36.08±4.74	136.03±20.64	28.39±4.32	1215.28±138.67	18.35±2.91	30.08±4.26	6.94±0.85

Table 146.X: Surface waviness as p–v and rms, collected with a 5× objective at the spots' ddp of three polycrystalline IR substrates. Data were obtained using a low-pass filter.

Sample	Acidic MR Fluid with Alumina Abrasive		Acidic MR Fluid with Nanodiamond Abrasive	
	p–v (nm)	rms (nm)	p–v (nm)	rms (nm)
HIP ZnS	331.37±84.21	58.52±14.01	379.21±13.35	58.35±3.04
ZnSe	377.94±21.65	53.06±0.71	236.33±83.42	29.31±6.67
MgF_2	45.69±8.01	5.76±1.33	9.81±0.75	4.84±4.15

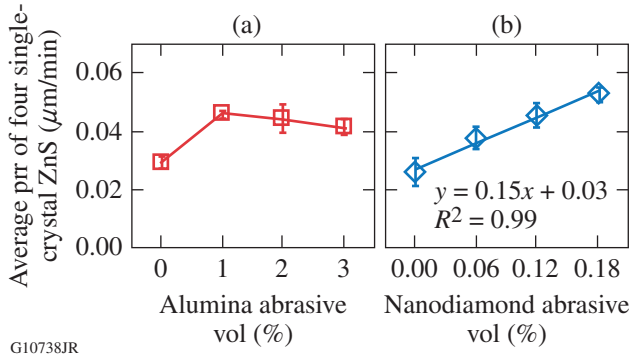

Figure 146.51
Average peak removal rate (prr) of all four single-crystal orientations versus abrasive concentration in the acidic MR fluid. (a) Alumina-based acidic MR fluid and (b) nanodiamond-based acidic MR fluid. Note that the alumina-abrasive concentration is ~10× higher than that of the nanodiamond abrasive.

For the next stage of the experiment—MRF of polycrystalline IR substrates—acidic formulations that contained the maximum amount of alumina and nanodiamond abrasives were used (i.e., a concentration of 3 vol % of alumina and 0.18 vol % of nanodiamonds).

2. Surface Finish of Polycrystalline CVD ZnS

The surface finish at the spots' ddp for all CVD ZnS samples (A–D) measured with 5× and 20× objectives is shown in Tables 146.VIII and 146.IX, respectively. Pebbles were studied using data from Table 146.VIII representing surface waviness (original roughness data are provided in **Appendix A**, p. 107). Surface microroughness was studied using data from Table 146.IX. Table 146.VIII indicates that the alumina-based acidic MR fluid produced less waviness on the surface of samples A and B than on samples C and D, in which the waviness was ~50% higher. When the samples were finished with a nanodiamond-based acidic MR fluid, similar surface waviness was observed for samples A and B. For samples C and D, however, the level of waviness is closer in value to that of samples A and B. Surface microroughness data in Table 146.IX show a similar trend to what was seen with surface waviness. When finished with an alumina-based acidic MR fluid, the microroughness of samples A and B was similar; the microroughness of samples C and D was similar, but ~40% higher than that of samples A and B. When the samples were finished with a nanodiamond-based acidic MR fluid, all samples showed a remarkable surface microroughness as a lineout of ~30-nm p–v and ~6-nm rms, and the large difference in roughness among samples A–D was diminished. A power spectral density (PSD) analysis of samples A–D, given in Fig. 146.52, also shows that MRF using the nanodiamond-based acidic MR fluid resulted in less pebbles on the surface and improved surface microroughness. At a spatial frequency below 100 mm^{-1} (corresponding to a lateral distance of 0.1 mm and higher), all CVD ZnS samples show a flatter and lower power density (PD) trend line. This indicates a reduction in pebbles on the surfaces that are finished with an acidic MR fluid containing nanodiamonds. At a spatial frequency above 100 mm^{-1} (a range that represents microroughness), samples A and B reach the lowest PD value, indicating that their microroughness is lower compared to samples C and D. Overall, the PSD results support the waviness and roughness analyses presented in Tables 146.VIII and 146.IX.

White-light interferometer micrographs taken with a 20× objective (given in Figs. 146.53 and 146.54) show the different

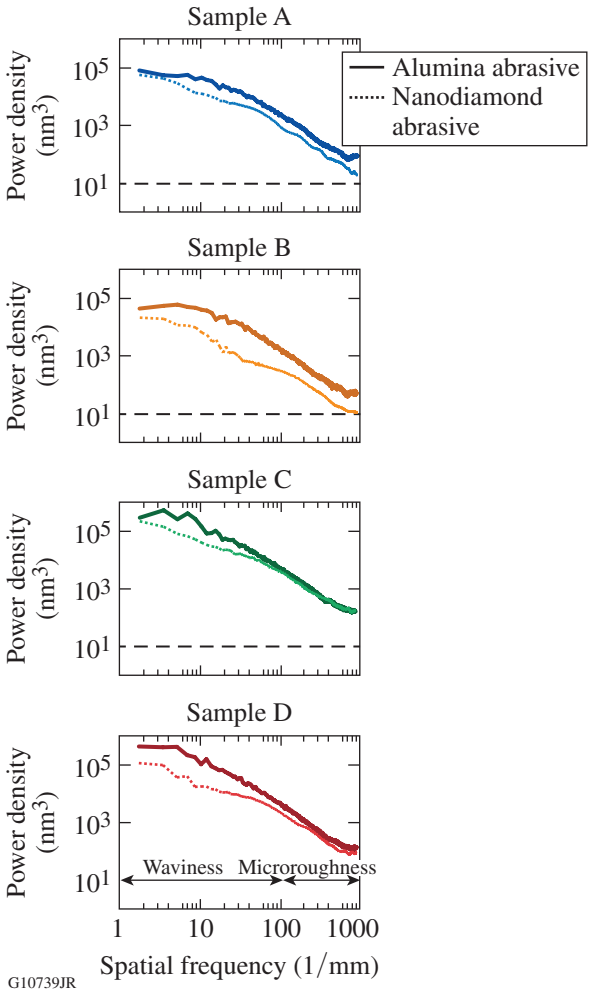

Figure 146.52
Power spectral density (PSD) for CVD ZnS samples A–D. The solid curves designate an acidic MR fluid with an alumina abrasive; the dotted curves designate acidic MR fluid with a nanodiamond abrasive.

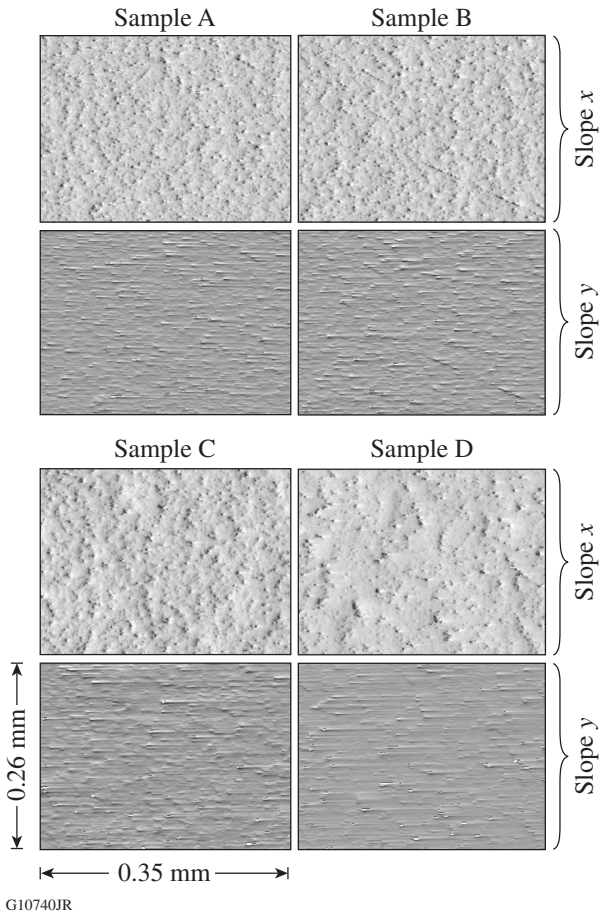

Figure 146.53
White-light interferometer (Zygo NewView™ 100) micrographs (20× objective; 0.35 × 0.26 mm^2) at the ddp of CVD ZnS samples A–D finished with an acidic MR fluid containing an alumina abrasive. The top micrographs designate "slope *x* surface maps;" the bottom micrographs designate "slope *y* surface maps." Pits on the surface (seen in the *x* slope maps) correspond to MR ribbon grooves (seen in the *y* slope maps) in the direction of the MR fluid flow.

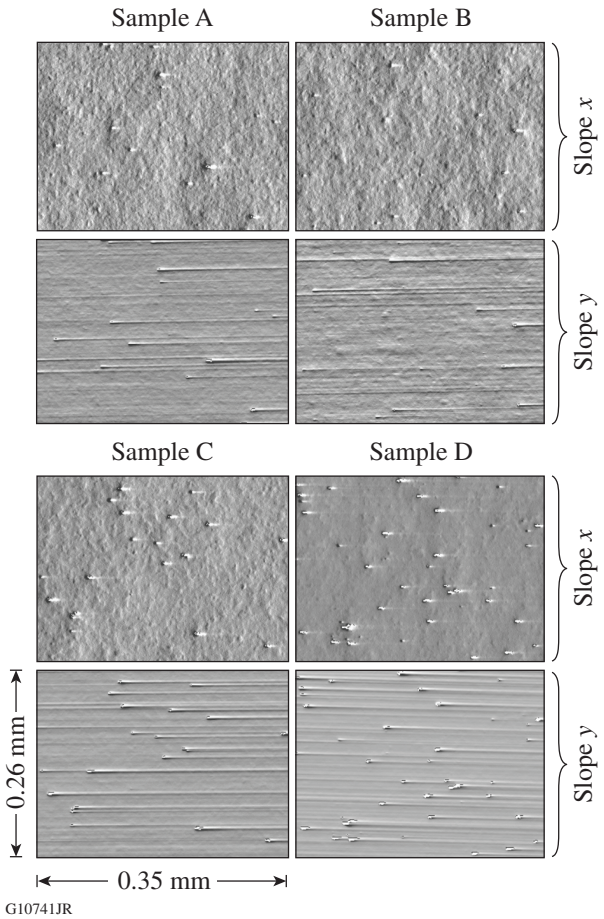

Figure 146.54
White-light interferometer (Zygo NewView™ 100) micrographs (20× objective; 0.35 × 0.26 mm^2) at the ddp of CVD ZnS samples A–D finished with an acidic MR fluid containing a nanodiamond abrasive. The top micrographs designate "slope *x* surface maps;" the bottom micrographs designate "slope *y* surface maps." Pits on the surface (seen in the *x* slope maps) correspond to MR ribbon grooves (seen in the *y* slope maps) in the direction of the MR fluid flow.

textures on surfaces finished with the two acidic MR fluids. For the alumina-based MR fluid (Fig. 146.53), a pitted pattern appears on all CVD ZnS samples (A–D). These pits seem to be a result of the grooves created by the MR ribbon in the direction of the MR fluid flow ("slope *y* surface map" micrographs in Fig. 146.53). A similar observation was found when nanodiamonds were used in the acidic MR fluid. In this case, however, the amount of pits and grooves is significantly lower, especially for samples A and B.

3. Surface Finish of Other Polycrystalline IR Optical Materials

The two acidic MR fluids used with polycrystalline, CVD ZnS substrates A–D, described in **Surface Finish of Polycrystalline CVD ZnS** (p. 103), were also used on CVD HIP ZnS, CVD ZnS, and MgF_2—which is not a CVD-grown material. Tables 146.X and 146.XI show the surface waviness and surface microroughness, respectively, of these materials (original data collected with a 5× objective are given in **Appendix A**, p. 107). Table 146.X indicates that CVD HIP ZnS and CVD ZnSe share similar values of waviness when finished with alumina-based acidic MR fluid. The pebbles on the surfaces are of the same order of magnitude. No change is seen in the emergence and size of pebbles on the CVD HIP ZnS surface when using nanodiamond abrasives instead of alumina in the acidic fluid. The surface waviness of CVD ZnSe, however, improves by ~40% when using a nanodiamond abrasive in the acidic MR fluid, indicating a reduction in the appearance of pebbles on the sur-

Table 146.XI: Surface microroughness as areal and lineout p–v and rms collected with a 20× objective at the spots' ddp of three polycrystalline IR substrates.

Sample	Acidic MR Fluid with Alumina Abrasive				Acidic MR Fluid with Nanodiamond Abrasive			
	Areal		Lineout		Areal		Lineout	
	p–v (nm)	rms (nm)	p–v (nm)	rms (nm)	p–v (nm)	rms (nm)	p–v (nm)	rms (nm)
HIP ZnS	1180.68±158.00	47.48±8.72	160.62±31.7	36.39±9.56	1476.20±251.10	58.80±15.90	191.30±57.67	54.30±20.60
ZnSe	1734.16±230.39	81.49±9.57	193.55±38.2	46.37±9.77	2270.10±351.85	66.80±8.31	87.39±26.31	21.20±5.72
MgF_2	554.91±142.89	7.72±0.72	38.81±5.881	6.68±0.75	43.54±12.72	1.32±0.13	6.06±0.92	1.09±0.18

face. Magnesium fluoride does not experience the pebble-like structure seen in CVD-grown materials. However, an ~80% improvement is seen in p–v and rms values of this material when using the acidic MR fluid with nanodiamond abrasives.

Surface microroughness results seen in Table 146.XI show that better surface roughness for the CVD HIP ZnS surface was obtained when an alumina abrasive was used in the acidic MR fluid. This is also seen in Figs. 146.55 and 146.56, in which the substrate's roughness is somewhat less pronounced and defined in Fig. 146.55 than in Fig. 146.56. When avoiding the MR ribbon grooves by taking roughness measurements as lineouts (see "Lineout" columns in Table 146.XI), a remarkable reduction in the p–v and rms values is observed. Overall, the alumina-based MR fluid provided better surface roughness for HIP CVD ZnS than the nanodiamond-based fluid.

The microroughness of CVD ZnSe finished with the acidic MR fluid and alumina abrasive is relatively high. A significant reduction in surface roughness, however, was found when this material was finished with nanodiamonds in the MR fluid.

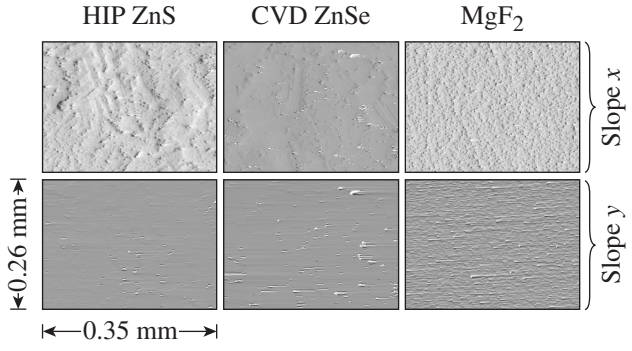

Figure 146.55
White-light interferometer (Zygo NewView™ 100) micrographs (20× objective; 0.35 × 0.26 mm^2) at the ddp of CVD HIP ZnS, CVD ZnSe, and MgF_2 finished with an acidic MR fluid containing an alumina abrasive. Pits on the surface (seen in the *x* slope maps) correspond to MR ribbon grooves (seen in the *y* slope maps) in the direction of the MR fluid flow.

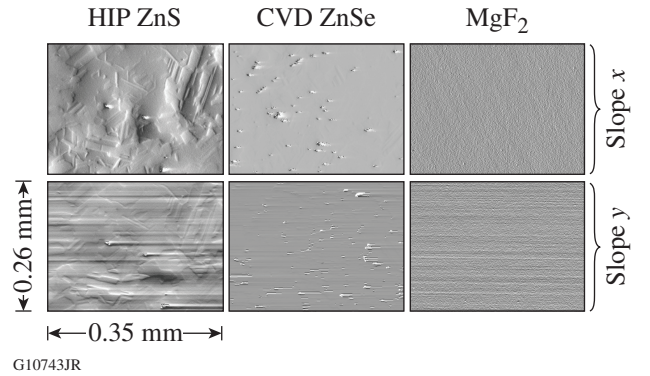

Figure 146.56
White-light interferometer (Zygo NewView™ 100) micrographs (20× objective; 0.35 × 0.26 mm^2) at the ddp of CVD HIP ZnS, CVD ZnSe, and MgF_2 finished with an acidic MR fluid containing a nanodiamond abrasive. Pits on the surface (seen in the *x* slope maps) correspond to MR ribbon grooves (seen in the *y* slope maps) in the direction of the MR fluid flow.

Figure 146.56 demonstrates the diminished small-scale pebbles on the surface of a CVD ZnSe substrate finished with an acidic MR fluid containing nanodiamonds. PSD data (Fig. 146.57) show similar observations. The power-density versus spatial-density plot of the surface finished with nanodiamonds shows significantly lower values than the alumina abrasive, indicating a reduction in the surface roughness (and pebbles) on the surface. For the MgF_2 substrate, finishing this material with an acidic MR fluid containing alumina provided a relatively good surface roughness (~38-nm p–v and ~7-nm rms as lineout). Roughness was significantly improved by more than 80% when using fluid containing nanodiamonds (~7-nm p–v and ~1-nm rms as lineout), with similar improvements in PSD results for this material obtained with the acidic MR fluid containing nanodiamonds being substantially better than that of an alumina-based MR fluid.

Discussion

Adding polishing abrasives to the acidic MR fluid increased the overall material removal rate of the fluid, while maintaining relatively good uniformity among the different single-crystal orientations of ZnS. Adding an alumina abrasive to the fluid

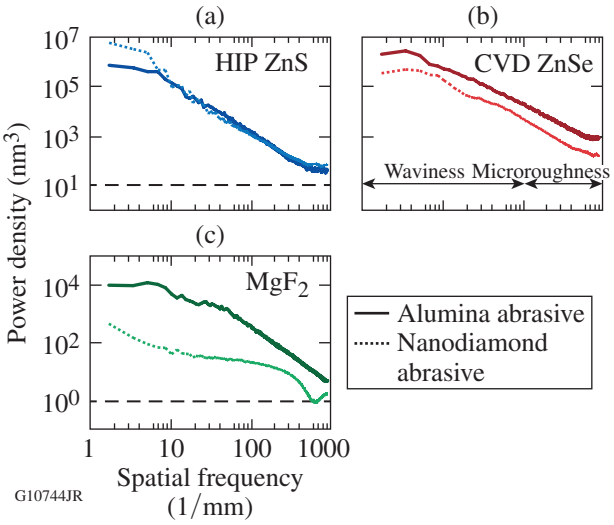

Figure 146.57
Power spectral density (PSD) for (a) CVD HIP ZnS, (b) CVD ZnSe, and (c) MgF_2 samples. The solid curves designate an acidic MR fluid with an alumina abrasive; the dotted curves designate an acidic MR fluid with nanodiamond abrasive.

caused saturation in the material removal rate with the first addition of a 1-vol % abrasive. With a nanodiamond abrasive, a constant increase in the material removal rate of ~18% was seen with any additional portion of abrasive. Surface waviness and PSD results show a significant reduction in the emergence of pebbles on the surface of several CVD ZnS substrates (samples A–D) finished with an acidic MR fluid containing nanodiamonds. The surface microroughness achieved was as low as ~30-nm p–v and ~6-nm rms. Furthermore, the variation in surface artifacts and roughness among the different CVD ZnS substrates, which is known to result from differences in detailed manufactory conditions of different suppliers,[30] was also resolved when a nanodiamond abrasive was used in the acidic MR fluid. The pronounced pits and MR grooves on the finished surfaces are believed to contribute to the overall roughness data collected and presented in this work. Since these grooves result from parts being stationary and not rotating during the process, we assume that lower roughness data, especially p–v, could be obtained if these surfaces were polished on a commercial MRF machine. The nanodiamond-based acidic MR fluid seemed to reduce the surface artifacts and microroughness of CVD ZnSe and MgF_2, but not those of CVD HIP ZnS. This finding was unexpected since CVD HIP ZnS is most similar to CVD ZnS; therefore, we would expect it to show similar surface waviness and roughness findings. This led us to the conclusion that the ceramic's crystallite (grain) size might have an effect on the resultant finish of the samples. Among the four types of polycrystalline evaluated here, CVD ZnS and MgF_2 have a smaller grain size. For these two materials, a good surface roughness and a minimal level of surface artifacts and pebbles were observed. The CVD ZnSe has an intermediate grain size (~45 μm) among the four evaluated materials. For this material some degree of surface artifacts and a surface microroughness of ~87-nm p–v and 21-nm rms were observed. The CVD HIP ZnS has the highest grain size of all four materials (~75 μm) because of the high temperature (~1000°C) reached during the HIP process, where recrystallization of the grains occurs.[22] With this material, a high degree of surface artifacts and pebbles was found on the MR-finished surface with both acidic fluids containing alumina and nanodiamonds. The surface microroughness was fairly high as well (>160-nm p–v and >36-nm rms). Further investigation of this assumption is required.

Conclusion

The addition of a polishing abrasive to the low-pH, low-viscosity MR fluid did not seem to affect the relative mrr among the different single-crystal orientations of ZnS. The overall mrr of the single-crystal orientations increased with an increasing nanodiamond concentration in the fluid but remained more or less the same when the concentration of alumina abrasives was increased. Surface-waviness and PSD results have shown that the emergence of pebbles on the surface of several CVD ZnS substrates (samples A–D) finished with the acidic MR fluid containing nanodiamonds was significantly reduced and the surface microroughness achieved was as low as ~30-nm p–v and ~6-nm rms. Furthermore, the variation in surface artifacts and microroughness among the different CVD ZnS substrates was also resolved with this type of abrasive in the acidic MR fluid. The pronounced pits and MR grooves observed on the finished surfaces contributed to the overall roughness data we collected; we believe that lower roughness data, particularly p–v, can be obtained if these surfaces were to go through a complete finishing run on a commercial MRF machine. The acidic MR fluid with nanodiamonds seemed to reduce the surface artifacts and microroughness of CVD ZnSe and MgF_2 but not that of CVD HIP ZnS. We speculate that the ceramic's grain size might have some influence in this matter. Further investigation is clearly required.

ACKNOWLEDGMENT

We thank Dr. S. Gorodkin and QED Technologies for their help and guidance with the surface waviness analysis using MetroPro software. This material is based upon work supported by the Department of Energy National Nuclear Security Administration under Award Number DE-NA0001944, the University of Rochester, and the New York State Energy Research and Development Authority. The support of DOE does not constitute an endorsement by DOE of the views expressed in this article. This work is synergistic with the NSF I/UCRC Center for Freedom Optics (IIP-1338877 and IIP-1338898).

Appendix A: White-Light Interferometer Roughness Data Collected with a 5× Objective

The data in Tables 146.XII and 146.XIII were used to perform the waviness analysis described in **Results** (p. 101).

Table 146.XII: Surface roughness (areal and lineout) collected with a 5× objective at the spots' ddp of four CVD ZnS substrates.

CVD ZnS Sample ID	Acidic MR Fluid with Alumina Abrasive				Acidic MR Fluid with Nanodiamond Abrasive			
	Areal		Lineouts		Areal		Lineouts	
	p–v (nm)	rms (nm)	p–v (nm)	rms (nm)	p–v (nm)	rms (nm)	p–v (nm)	rms (nm)
Sample A	287.56±180.42	13.42±2.00	72.93±12.18	12.56±1.16	525.96±177.97	12.53±0.91	55.78±12.35	10.64±2.53
Sample B	737.48±486.54	15.12±2.32	76.91±13.84	13.60±1.46	360.24±10.53	8.21±0.45	36.27±7.01	7.08±0.94
Sample C	1292.91±1241.49	29.37±0.94	146.63±19.77	26.98±2.10	379.23±27.48	10.46±2.13	39.90±5.40	7.99±1.08
Sample D	918.48±599.05	36.52±0.76	184.47±27.50	32.05±5.13	529.31±155.43	11.85±3.54	50.42±9.49	9.19±1.74

Table 146.XIII: Surface roughness (areal and lineout) collected with a 5× objective at the spots' ddp of CVD HIP ZnS, CVD ZnSe, and MgF_2.

Sample	Acidic MR Fluid with Alumina Abrasive				Acidic MR Fluid with Nanodiamond Abrasive			
	Areal		Lineouts		Areal		Lineouts	
	p–v (nm)	rms (nm)	p–v (nm)	rms (nm)	p–v (nm)	rms (nm)	p–v (nm)	rms (nm)
HIP ZnS	1254.13±641.29	72.67±14.50	290.56±60.10	65.26±18.10	868.02±47.76	71.70±2.95	262.40±53.54	62.90±10.40
ZnSe	1528.77±784.67	74.25±1.96	308.96±43.77	68.19±10.90	1714.70±0.76	46.70±5.98	178.90±31.38	36.00±7.02
MgF_2	237.10±1.55	8.33±1.55	46.06±8.35	7.81±1.31	37.89±4.85	2.16±0.15	7.19±1.59	1.22±0.29

REFERENCES

1. S. D. Jacobs, D. Golini, Y. Hsu, B. E. Puchebner, D. Strafford, Wm. I. Kordonski, I. V. Prokhorov, E. Fess, D. Pietrowski, and V. W. Kordonski, Proc. SPIE **2576**, 372 (1995).
2. S. D. Jacobs, S. R. Arrasmith, I. A. Kozhinova, L. L. Gregg, A. B. Shorey, H. J. Romanofsky, D. Golini, Kordonski. W. I., P. Dumas, and S. Hogan, in *Finishing of Advanced Ceramics and Glasses*, edited by R. Sabia, V. A. Greenhut, and C. G. Pantano, Ceramic Transactions, Vol. 102 (The American Ceramic Society, Westerville, OH, 1999), pp. 185–199.
3. J. E. DeGroote, H. J. Romanofsky, I. A. Kozhinova, J. M. Schoen, and S. D. Jacobs, Proc. SPIE **5180**, 123 (2003).
4. S. N. Shafrir, J. C. Lambropoulos, and S. D. Jacobs, J. Manuf. Sci. Eng. **129**, 961 (2007).
5. D. Golini, in *Precision Science and Technology for Perfect Surfaces*, edited by Y. Furukawa, Y. Mori, and T. Kataoka, JSPE Publication Series No. 3 (The Japan Society for Precision Engineering, Tokyo, Japan, 1999), pp. 132–137.
6. M. Beier *et al*., Proc. SPIE **8884**, 88840S (2013).
7. *LLE Review Quarterly Report* **80**, 213, Laboratory for Laser Energetics, University of Rochester, Rochester, NY, LLE Document No. DOE/SF/19460-321, NTIS Order No. DE00761211 (1999).
8. S. D. Jacobs, F. Yang, E. M. Fess, J. B. Feingold, B. E. Gillman, W. I. Kordonski, H. Edwards, and D. Golini, Proc. SPIE **3134**, 258 (1997).
9. I. A. Kozhinova, H. J. Romanofsky, A. Maltsev, S. D. Jacobs, W. I. Kordonski, and S. R. Gorodkin, Appl. Opt. **44**, 4671 (2005).
10. B. Hallock *et al*., in *Frontiers in Optics 2008/Laser Science XXIV/Plasmonics and Metamaterials/Optical Fabrication and Testing*, OSA Technical Digest (CD) (Optical Society of America, Washington, DC, 2008), Paper OThB2.
11. "Calcium Fluoride Properties (CaF_2)," ISP Optics, Irvington, NY, 10533, http://www.janis.com/Libraries/Window_Transmissions/CalciumFluoride_CaF2_TransmissionCurveDataSheet.sflb.ashx.
12. J. A. Menapace, P. R. Ehrmann, and R. C. Bickel, Proc. SPIE **7504**, 750414 (2009).
13. L. N. Pattanaik and H. Agarwal, Int. J. Adv. Mech. Eng. **4**, 611 (2014).
14. L. L. Gregg, A. E. Marino, J. C. Hayes, and S. D. Jacobs, Proc. SPIE **5180**, 47 (2004).
15. J. D. Nelson *et al*., Proc. SPIE **8708**, 870815 (2013).
16. M. Brophy, J. D. Nelson, and T. Hordin, in *Classical Optics 2014*, OSA Technical Digest (online) (Optical Society of America, Kohala Coast, Hawaii, 2014), Paper OW3B.3.
17. I. Kozhinova, S. R. Arrasmith, J. C. Lambropoulos, S. D. Jacobs, and H. J. Romanofsky, Proc. SPIE **4451**, 277 (2001).
18. C. Supranowitz *et al*., Proc. SPIE **6545**, 65450S (2007).
19. S. Salzman, H. J. Romanofsky, Y. I. Clara, L. J. Giannechini, G. West, J. C. Lambropoulos, and S. D. Jacobs, Proc. SPIE **8884**, 888407 (2013).
20. J. McCloy *et al*., Proc. SPIE **8016**, 80160I (2011).
21. W. D. Callister, *Materials Science and Engineering*, 2nd ed. (Wiley, New York, 1991), pp. 131–141.

22. J. S. McCloy and R. W. Tustison, *Chemical Vapor Deposited Zinc Sulfide*, Vol. PM237 (SPIE, Bellingham, WA, 2013).

23. E. M. Gavrishchuk *et al*., Inorg. Mater. **43**, 579 (2007).

24. R. Shen, H. Yang, S. N. Shafrir, C. Miao, M. Wang, J. Mici, J. C. Lambropoulos, and S. D. Jacobs, U.S. Patent No. 8,808,568 B2 (19 August 2014).

25. S. N. Shafrir, H. J. Romanofsky, M. Skarlinski, M. Wang, C. Miao, S. Salzman, T. Chartier, J. Mici, J. C. Lambropoulos, R. Shen, H. Yang, and S. D. Jacobs, Appl. Opt. **48**, 6797 (2009).

26. R. Shen, S. N. Shafrir, C. Miao, M. Wang, J. C. Lambropoulos, S. D. Jacobs, and H. Yang, J. Colloid Interface Sci. **342**, 49 (2010).

27. L. J. Giannechini, "Design and Quantification of Highly Corrosion-Resistant Magnetorheological Finishing Powder," M.S. thesis, University of Rochester, 2015.

28. S. Salzman, L. J. Giannechini, H. J. Romanofsky, N. Golini, B. Taylor, S. D. Jacobs, and J. C. Lambropoulos, Proc. SPIE **9633**, 963307 (2015).

29. SurfaceNet GmbH, Landersumer Weg 40, D-48431 Rheine, Germany.

30. S. Salzman, H. J. Romanofsky, S. D. Jacobs, and J. C. Lambropoulos, Prec. Eng. **43**, 257 (2016).

31. J. A. Salem, National Aeronautics and Space Administration, Glenn Research Center, Cleveland, OH, Report NASA/TM—2006-214100 (2006).

32. T.-C. Wen and D. K. Shetty, Proc. SPIE **7302**, 73020Z (2009).

33. Colloidal Dynamics, Ponte Vedra Beach, FL 32082.

34. Zygo Mark IVxp™, Zygo Corporation, Middlefield, CT 06455-1291, http://www.zygo.com (25 May 2016).

35. J. S. Goela and R. L. Taylor, J. Mater. Sci. **23**, 4331 (1988).

36. K. L. Lewis *et al*., in *Proceedings of the Ninth International Conference on Chemical Vapor Deposition 1984*, edited by Mc. D. Robinson *et al*. (Electrochemical Society, Pennington, NJ, 1984), pp. 530–545.

37. NewView™ 100, White Light Optical Profiler (areal over 0.26 mm × 0.35 mm with a 20× Mirau objective, no filter) by Zygo Corporation, Middlefield, CT 06455-1270, http://www.zygo.com (25 May 2016).

38. G. West, "Measuring Surface Texture in MRF Spots on Polycrystalline Material," LLE Internal Memorandum, Laboratory for Laser Energetics, University of Rochester, Rochester, NY (3 August 2011).